2022

The Role of Internal Heat Exchanger in an R744 Vapor Compression System in the Heat Pump Mode Under Various Conditions

Vladimir Cernicin

Wenying Zhang

Pega Hrnjak

The Role of Internal Heat Exchanger in an R744 Vapor Compression System in the Heat Pump Mode Under Various Conditions

Vladimir CERNICIN [1], Wenying ZHANG [2], Pega HRNJAK[2, 3]*

[1]Faculty of Mechanical Engineering, University of Belgrade, Belgrade, Serbia
vcernicin@mas.bg.ac.rs

[2]ACRC, University of Illinois, Urbana, Illinois, USA
wenying3@illinois.edu

[3]Creative Thermal Solutions, Inc., Urbana, Illinois, USA
pega@illinois.edu

* Corresponding Author

ABSTRACT

In this paper, the role of the internal heat exchanger (IHX) in a reversible R744 vapor compression system in the heating mode was investigated experimentally and presented. At the first, the optimal refrigerant charge amount for both basic and the IHX systems was determined. Also, the control equations of HPF-maximizing high side pressure were developed and used for both systems. Then, well-tuned systems working at the optimal discharge pressure were compared in two scenarios under various conditions. The results of the experiments reveal the potential benefits of introducing IHX for the R744 system in the heating mode. The efficiency was improved by up to 10.5% by introducing the internal heat exchanger. Also, the benefits of IHX in the frosting conditions were discussed.

1. INTRODUCTION

One of the basic measures to increase the cooling capacity in order to improve the efficiency of the refrigeration system is the subcooling method. The essential is to subcool the liquid refrigerant leaving the condenser either using the other liquid (external subcooling method) or using the same refrigerant at the evaporator exit (internal subcooling method). External subcooling method is always beneficial for efficiency, but rarely available. On the other hand, the internal subcooling method using the internal heat exchangers (IHXs) is widely applied in the refrigeration and heat pump systems. However, the potential efficiency improvement depends on the tradeoff between the increase of the specific cooling capacity and the increase of specific work. This tradeoff, from a simple cycle analysis point of view, will have a direct and bigger effect on the refrigeration system than on the heat pump system. For that reason, it is expected for heat pump systems to work similarly with and without IHX, and therefore refrigeration systems receive more attention in the open literature.

The more detailed analysis is based on the system modelling and for that reason several papers are mentioned. Kim et al. (2005) investigated the performance of a transcritical CO_2 water heater system with a IHX numerically. Also, the efficiency of the system is slightly improved by introducing an IHX up to certain discharge pressure. Ghazizade-Ahsaee and Ameri (2018) investigated numerically the effects of using expander and IHX in a horizontal Direct-Expansion Geothermal Heat Pump (DX-GHP). The authors concluded that using an IHX in the cycle with expansion valve always leads to a slight increase in the efficiency and the exergy efficiency. In the cycle with expander there is no significant effect. Nguyen et al. (2019) analyzed the influence of an IHX on the similar system with vertical loop through transient energy simulations. They showed that adding IHX to the system effectively counters the effect of thermal short-circuiting in the borehole as well as ground surface temperature variations, and increases its efficiency. Kwan et al. (2020) set the thermoelectric device as IHX and system efficiency was improved by 5% in their simulation. Ye et al. (2020) developed a theoretical model that considered the pinch point in a gas cooler and the application of IHX. Introduction of IHX, regardless of the working condition, lowered the optimal discharge

pressure and enhanced corresponding optimal COP. It was concluded that reduction of the optimal discharge pressure could be up to 1.18 MPa when the effectiveness of IHX was 0.6. The similar conclusions were brought by Wang et al. (2021) in their energy, exergy and exergoeconomic study. Also, with adding IHX, the irreversibility of the throttling valve is greatly reduced by 40.36% - 50.73%.

Fernandez et al. (2010) investigated the overall efficiency during full tank heating tests. The performance enhancement caused by using IHX was up to 7.9% for initial tank water heating and around 3.4% for reheating a warm tank water. As an example of refrigerant that always works in subcritical mode, Ortega et al. (2019) presented the experimental study of R407C liquid-to-water heat pump for combined space heating and domestic hot water. Application of IHX yields lower heating capacity and compression power, and therefore slightly lower efficiency. Cao et al. (2020) conducted an experimental study on the transcritical CO2 heat pump water heater prototype. The IHX reduces the total power consumption by up to 6.22% and improves the system efficiency by up to 6.65%. Also, application of IHX increases the exergy destruction of the compressor, gas cooler and evaporator, and reduces the exergy efficiency of the system. Qin et al. (2021) investigated the effect of IHX based on the actual operation thermal effectiveness and the actual increase rate of efficiency. They showed that the actual increase rate of Coefficient of Performance (COP) can effectively evaluate the impact of the IHX on system performance.

Jung et al. (2020) proposed R134a vapor injection heat pump for electric vehicles to improve the performance and reliability. In addition, the effect of the IHX length and the different injection-port angle was analyzed. For the maximum efficiency of the system, the optimum IHX length and injection-port angle was determined to be 300 mm and 400°. Junqi et al. (2021) analyzed R134a and R744 heat pump systems working in both modes (AC/HP). The R744 HP system works with an accumulator with internal heat exchanger (Acc/IHX), which has beneficial effects for its work.

Although the effects of IHX on the performance of a transcritical CO_2 heat pump system have been studied by different researchers, the role of an IHX in a reversible CO_2 AC/HP system has not been discussed in public literature. In this paper and an accompanying paper (Zhang et al., 2022), the role of IHX in both HP and AC modes will be discussed with an experimental illustration of an R744 system under various conditions. The influence of refrigerant charge amount, efficiency-maximizing control equation, and normalized heating performance will be presented. The conclusion can be used to guide the design of reversible R744 heat pump systems for different applications.

2. EXPERIMENTAL SETUP

2.1 Facility

In this paper, the effect of IHX on the R744 air-source HP system was investigated experimentally. For this purpose, a facility with two climate chambers was calibrated. **Figure 1** presents the reversible R744 heat pump system inside and between the climate chambers with the following refrigerant-side sensors. The one-slab two-pass outdoor coil (evaporator in HP mode) and the Electronic Expansion Valve (EXV) for HP mode were installed inside the outdoor climate chamber. The two-slab four-pass indoor coil and the EXV for AC mode were installed inside the indoor climate chamber. The circuit between two chambers consists of a semi-hermetic reciprocating compressor, the accumulator (Acc) with integrated internal heat exchanger (IHX), and the EXV controllers. For basic system (without IHX) investigation, IHX is bypassed using the ball valves 5 and 6 on the high side. The whole system could be easily reversed from HP mode to AC mode by controlling the ball valves 1 to 4. The valves depicted in black are closed, while those depicted in white are open. The reversed system was investigated in the accompanying paper (Zhang et al., 2022) and the dimensions of the key components are listed in it.

Different conditions in both climate chambers were set up and maintained with a glycol heat exchanger, a PID-controlled electric heater, and a wind tunnel with VFD-controlled blowers installed in each of them. To measure the temperature, humidity, and airflow rate, thermocouple grids, dew point sensors, air nozzles, and differential pressure transducers were installed in the wind tunnels.

To measure consumed energy inside the climate chamber, power transducers were used. The cooling capacity of the glycol heat exchangers was calculated using measured glycol mass flow rates and inlet/ exit glycol temperatures for both chambers. Using the chamber-side energy balance, the heat loss through the insulation walls, the heating/

cooling capacity of indoor/ outdoor coils were calculated. Outside of the chambers, as shown in **Figure 1,** pressure transducers, thermocouple probes, and a mass flow meter were installed to cover the rest of the measuring points.

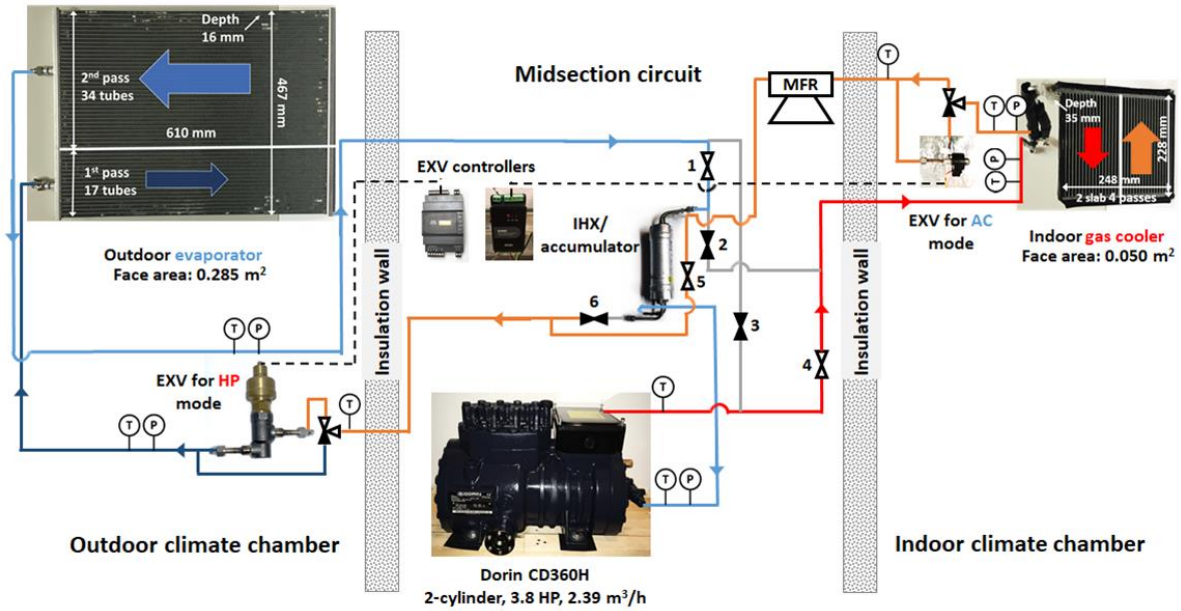

Figure 1: Schematic drawing of the R744 system in HP mode

All sensors were calibrated prior installed in the facility. The details and uncertainties of the sensors are listed in the accompanying paper (Zhang et al., 2022). The signals from the sensors are measured by an HP series 75000B data logger and converted to SI-unit parameters via the VEE program. For each condition, we waited for at least 30 minutes to stabilize the reading and then recorded the data for another 20 minutes with an interval of 6 seconds.

2.2 Data reduction and uncertainty analysis

The heating/ cooling capacities of indoor/ outdoor coil in the R744 system with and without IHX were calculated using refrigerant-, air-, and chamber-side balances. The thermodynamic properties were calculated using commercial software- Refprop 9.0 (Lemmon. et al., 2010). For the indoor gas cooler, the three balances are shown below:

$$Q_{heating,ref} = (1-OCR)\dot{m}_r(h_{cri}-h_{cro}) + OCR\cdot\dot{m}_r(h_{coi}-h_{coo}) \quad \textbf{Eqn (1)}$$

$$Q_{heating,air} = \dot{m}_{cai,dry}(h_{cao}-h_{cai}) \quad \textbf{Eqn (2)}$$

$$Q_{heating,cham} = \dot{m}_{id,g}(T_{id,go}-T_{id,gi}) - (\sum P_{id,elec} + Q_{id,loss}) \quad \textbf{Eqn (3)}$$

Where OCR is the Oil Circulation Rate and was measured by the sampler installed across the mass flow meter on the liquid line. In this project, the OCR is measured to be 2% and the effects on system capacity are negligible. Mass flow $\dot{m}_r$ was measured by the mass flow meter, and it is actually the mass flow rate of the oil and CO_2 mixture. Refrigerant enthalpy h_{cri}, oil enthalpies h_{coi} and h_{coo} were determined from the pressures and temperatures measured at the inlet (T_{cri} and P_{cri}) and outlet (T_{cro} and P_{cro}) of the indoor coil. For the transcritical cycle, refrigerant enthalpy h_{cro} was determined from T_{cro} and P_{cro}.

The indoor air mass flow rate $m_{cai,dry}$ was calculated using measured air temperature (T_{can}), dew point (T_{dpcn}), and pressure drop (DP_{cn}) at the indoor nozzles. The enthalpies of air h_{cai} and h_{cao} were determined using air temperatures at the indoor coil inlet T_{cai} and exit T_{cao}. In the calculation, dry air properties were used because dew point measurements showed there was no water condensation across the indoor coil.

The electrical power consumption $P_{id,elec}$ of each device inside the indoor chamber was measured using power transducers. The heat loss through the insulation wall $Q_{id,loss}$ was calculated using the measured UA value of the

climate chamber. The mass flow rate of glycol flowing into the indoor chamber $m_{id,g}$ and the inlet and exit glycol temperatures ($T_{id,gi}$ and $T_{id,go}$) were used to calculate the cooling capacity of the glycol heat exchanger.
Similarly, three approaches were used to calculate the cooling capacity of the outdoor evaporator：

$$Q_{cooling,ref} = (1-OCR)\dot{m}_r(h_{ero} - h_{eri}) + OCR \cdot \dot{m}_r(h_{eoo} - h_{eoi}) \quad \textbf{Eqn (4)}$$

$$Q_{cooling,air} = \dot{m}_{eai,dry}(h_{eai} - h_{eao}) \quad \textbf{Eqn (5)}$$

$$Q_{cooling,cham} = \sum P_{od,elec} + Q_{od,loss} - \dot{m}_{od,g}(T_{od,go} - T_{od,gi}) \quad \textbf{Eqn (6)}$$

Also, for the IHX cycle, the capacity of the IHX was calculated using the high-leg refrigerant-side, since it is in the supercritical or subcooled zone:

$$Q_{IHX,ref} = (1-OCR)\dot{m}_r(h_{cro} - h_{xri}) + OCR \cdot \dot{m}_r(h_{coo} - h_{xoi}) \quad \textbf{Eqn (7)}$$

Where, refrigerant enthalpy h_{xri} and oil enthalpy h_{xoi} were determined from the pressure and temperature measured at the inlet of the expansion valve. The low-leg capacity of IHX equals the high-leg capacity, assuming no heat loss to the ambient.

The Heating Performance Factor (HPF) of the R744 heat pump system with and without IHX was calculated as:

$$HPF = \frac{Q_{heating,ave}}{P_{comp}} \quad \textbf{Eqn (8)}$$

Where, $Q_{heating,ave}$ is the average of ref-, air-, and chamber-side heating capacity of indoor gas cooler. P_{comp} is the measured electrical power consumption of the VFD-controlled compressor.

The uncertainty analysis was conducted using a MATLAB program integrated with the data reduction program, following the method of Moffat (1988). According to the method, the uncertainty in a calculated value R, which is a function of N independent measurements (X_1, X_2, X_3, ... X_N), can be calculated as **Eqn (9)**:

$$\delta R = \left(\sum_{i=1}^{N} \left(\frac{\partial R}{\partial X_i} \delta X_i \right)^2 \right)^{\frac{1}{2}} \quad \textbf{Eqn (9)}$$

Where uncertainty of each measurement is determined using **Eqn (10):**

$$\delta X_i = \left(\delta X_{i,A}{}^2 + \delta X_{i,B}{}^2 \right)^{\frac{1}{2}} \quad \textbf{Eqn (10)}$$

Where, $\delta X_{i,A}$ is the type-A uncertainty of measurement X_i, which was calculated as the standard deviation of each group of data recorded every 20 minutes. The type-B uncertainty $\delta X_{i,B}$ was either provided by the manufacturer or by the calibration: it is ±0.2℃ for the refrigerant temperatures after we calibrated the type-T thermocouples with RTD sensors (PT100). For the indoor heating capacity and HPF of the system, the average uncertainties that include ref-, air-, and chamber-side approaches were 6.9% and 8.1%, respectively.

3. RESULTS AND DISCUSSION

In this paper, the role of IHX in an R744 heat pump system operating in transcritical mode was studied experimentally. To compare the performance of the system with and without the IHX, the two groups of experiments were conducted to determine optimal refrigerant charge amounts and the efficiency-maximizing control equations for both basic and IHX systems. Then, both well-tuned systems were compared and analyzed in the next two steady-state scenarios under different conditions. Also, for those two groups of experiments, the effect of the

IHX on the performance of the HP system during frosting conditions was analyzed. For all of the experiments, despite the unrealistic conditions, relative humidity in the outdoor chamber was kept the same (RH_{eai} = 40%) to prevent the frosting of the outdoor coil. **Table** lists all the experimental conditions in this paper. The details and the results will be discussed in the following chapter.

Table 1: Operating conditions of all experiments in this paper

	The purpose of this group	T_{eai} **[°C]**	RH_{eai} **[%]**	V_{eai} **[m/s]**	T_{cai} **[°C]**	m_{cai} **[kg/min]**	**Compressor speed [%]**
Group 1	Optimal charge	0	40	3.0	10	6.0	80
Group 2	Control equations	-5/0/10			20		50 to 75
Group 3	Steady-state scenarios	-10/-5/0/5/10			20		Various values to match T_{cao} = 50 °C
Group 4	Warm-up scenarios	5			5/10/15/20		Various values to match $T_{cao} = T_{cai}$ + 30 °C

3.1 Effects of refrigerant charge amount on the system performance (Group 1)

The effects of the refrigerant charge amount on the R744 heat pump system with and without IHX are presented in the section. **Figure 2(a)** and **(b)** show the heating capacity, compressor power consumption, and HPF for the basic system and IHX system as the charge amount increases. **Figure 2(c)** and **(d)** present the refrigerant mass flow rate, pressure, and temperature of the refrigerant at different locations of each system during the charging experiments.

The temperatures for ambient and in-cabin air were kept the same (T_{eai} = 0°C, T_{cai} = 10°C). The humidity in the outdoor chamber was controlled to prevent frosting on the evaporator surface. The outdoor air velocity was 3.0 m/s, and the in-cabin air flow rate was 6.0 kg/min in the charging experiments. The compressor speed was fixed at 80% of the full speed (1450 rpm). During the charging procedure, CO_2 was added to the system in front of the Acc/IHX in increments of 50g and then stabilized for at least 30 minutes before recording data for another 20 minutes. For each charge amount, at least three different high-side pressures were tested to find the COP-maximizing pressure, which is presented in **Figure 2(c)** and **(d)** as P_{cro}.

For the basic system, the heating capacity $Q_{heating}$ and compressor power consumption W_{comp} increase as the refrigerant charge amount increases and reach a maximum of 1000 g. After that, both parameters start decreasing, but heating capacity is more sensitive to charge amount when the system is overcharged. However, due to similar trends in both parameters, HPF has a small plateau from 850 to 1000 g, as shown in **Figure 2(a)**. The system with IHX is less sensitive to the charge amount. In the other words, the heating capacity of the IHX system is more stable than it is for the basic system even when IHX system is undercharged. The plateau for heating capacity, compressor power consumption, and HPF is from 850 to 1050 g, as shown in **Figure 2(b)**. Now, the system is well charged and a two-phase refrigerant enters the accumulator. With the last point, the accumulator is flooded, and superheat decreases.

At the beginning of the charging experiments for both systems, the gas cooler exit temperature T_{cro} is low, and that is beneficial for heating capacity. For an undercharged system, mass flow rate m_r and high-side pressure P_{cro} are lower, and the limitations in compressor work (high T_{cpro}) are easier to achieve. With adding more charge amount, those parameters start to increase, T_{cpro} decreases, and m_r has more effect on the heating capacity and HPF than T_{cro}. The sensitivity of those parameters is the main difference in the system with and without IHX. For a basic system, all of the parameters are changing very fast with every charge amount, while for an IHX system it is easier to keep constant value. For example, the mass flow rate for the whole amount range increases two times for the basic system, but for the IHX system increases just 12%, as shown in **Figure 2 (c)** and **(d)**. To avoid sending too much liquid refrigerant into the compressor, another limitation (except high T_{cpro}) is the superheat at the compressor suction, For that reason, the basic system is very limited to further adding refrigerant due to constant decrease of the superheat on the evaporator outlet SH_{ero} and compressor inlet SH_{cpri}.

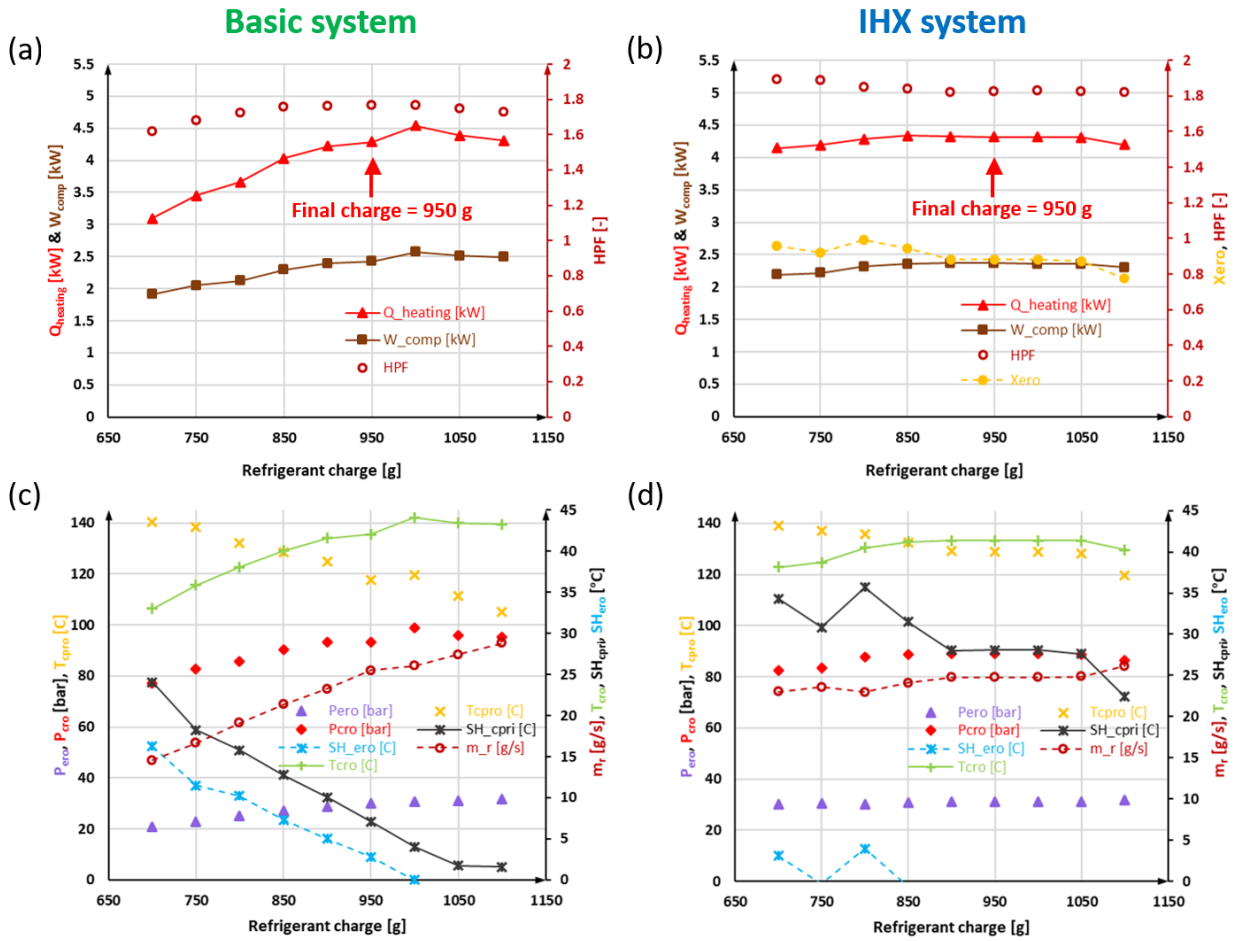

Figure 2: Results of charging experiments for the basic and IHX HP systems

Finally, the refrigerant charge amount was optimized to be 950 g for the basic system to avoid too much liquid refrigerant entering the reciprocating compressor. In the meanwhile, 950 g is also chosen for the IHX system, because liquid refrigerant is stored in the accumulator and the performance becomes stable starting at this point. Comparing the performance of both systems with the final charge, introducing IHX keeps the $Q_{heating}$ almost the same and improves HPF by 2.8% at the test condition. From this point of view, adding IHX provides not significant benefits on heating capacity and efficiency. However, it provides much more stable work of the system.

3.2 Effects of IHX on the control equations (Group 2)

To achieve the optimal system performance in a wide range of operating temperatures, control equations, instead of a fixed EXV opening, were developed for both basic and IHX systems to maximize efficiency. The high-side pressure control theory was discussed in detail and a graphical method was developed using ideal cycle analysis in the paper of Inokuty (1928) for AC mode. Due to the trade-off between the specific cooling capacity and specific compressor work, there exists one COP-maximizing high-side pressure for a fixed refrigerant gas cooler exit temperature. A similar rule should exist for HPF-maximizing high-side pressure in the HP mode. For that reason, the same logic and procedure was applied in HP mode, too.

Figure 3(a) and **(b)** show the HPF curves as functions of the refrigerant pressure at the gas cooler exit P_{cro} for the basic and IHX systems. The control variables including the operating temperatures, airflow rates (AFRs), charge amounts, and compressor speeds are listed in the charts. The maximum HPF and related T_{cro} are highlighted in red and then used to develop the control equations for both systems, as presented in **Figure 3(c)**. Both basic and IHX systems operating in transcritical mode reach the maximum efficiency at the lower high-side pressure and lower T_{cro}.

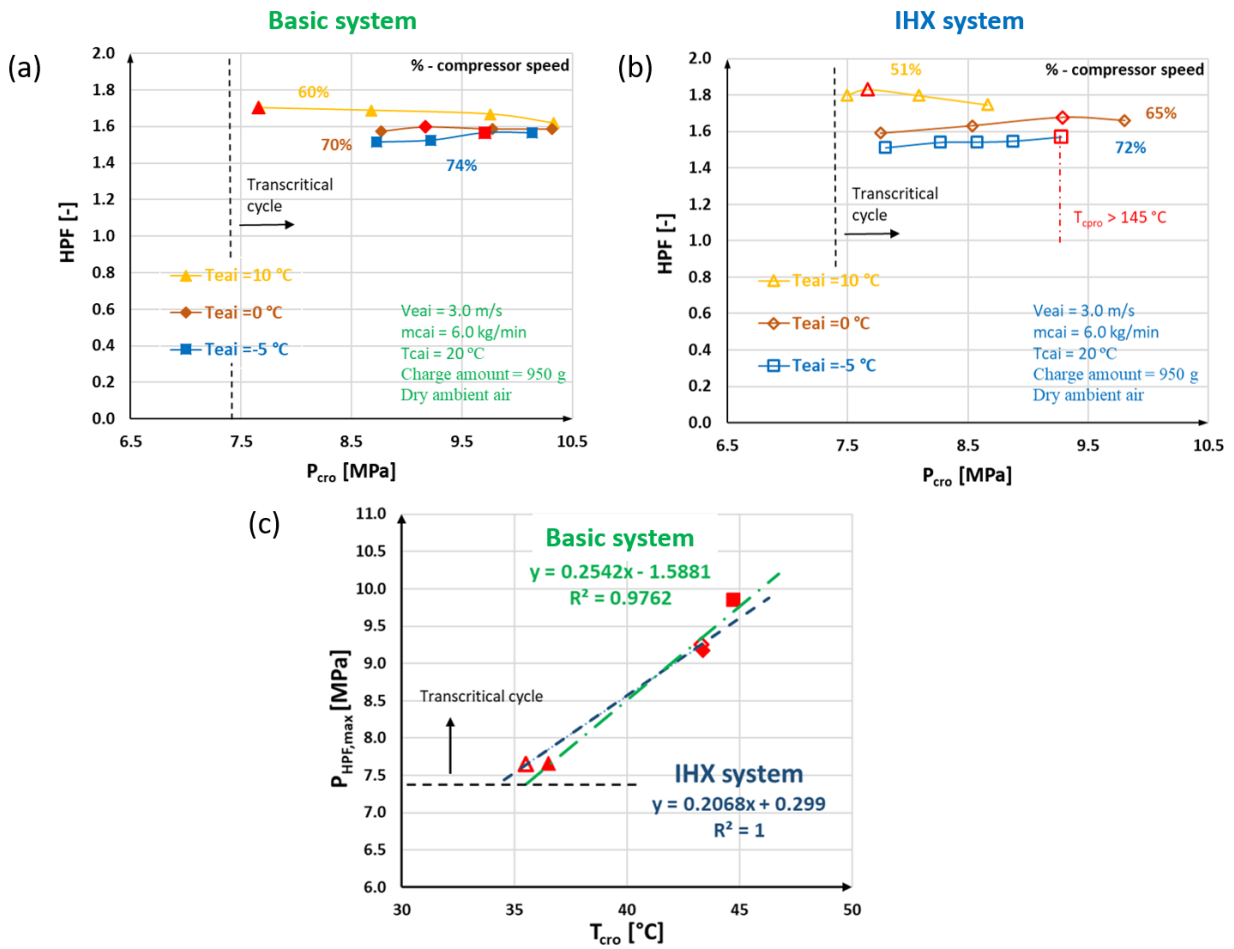

Figure 3: The performance data and high-side pressure control equations for the basic and IHX HP systems

The results show that HPF-maximizing control equations could be limited by the discharge temperature of the compressor, especially in high lift conditions (when Teai = -5°C). Overall, the deviation between the control equations is smaller in HP than it is in AC mode. Because the airflow rate and the air inlet temperature are relatively fixed for the indoor gas cooler. The IHX changes the slope of the $P_{HPF,max} - T_{cro}$ line, and after some point, the basic system demands higher HPF-maximizing pressure for higher gas cooler exit temperatures.

3.3 Effects of IHX on the HP system performance under various conditions (Group 3 and 4)

After fine-tuning the basic and IHX systems, we conducted experiments in the steady-state and warm-up scenarios to investigate the role of IHX in an R744 HP system. In the steady-state scenario, the indoor air inlet (T_{cai}) and exit (T_{cao}) temperatures are fixed to be 20 and 50°C (fixing the heating capacity), while the ambient air temperature T_{eai} varies from -10 to 10°C, with increments 5°C. In the warm-up scenario, T_{eai} is 5°C, T_{cai} changes from 5 to 20°C, and the indoor air exit temperature T_{cao} is always 30°C higher than T_{cai}. The compressor speed is adjusted to match the heating capacity, and all other control parameters are listed in the charts in **Figure 4**.

Figure 4 (a) and **(b)** show the experimental results of the HPF of both basic and IHX systems and the HPF improvement by introducing IHX. For low ambient temperature conditions (T_{eai}= -10°C), a system with IHX has lower efficiency due to compressor limitations of high discharge temperature. By increasing the ambient temperature for the steady-state scenario and increasing the indoor air inlet for the warm-up scenario, IHX improves the system efficiency by up to 9.8% and 10.5%, respectively.

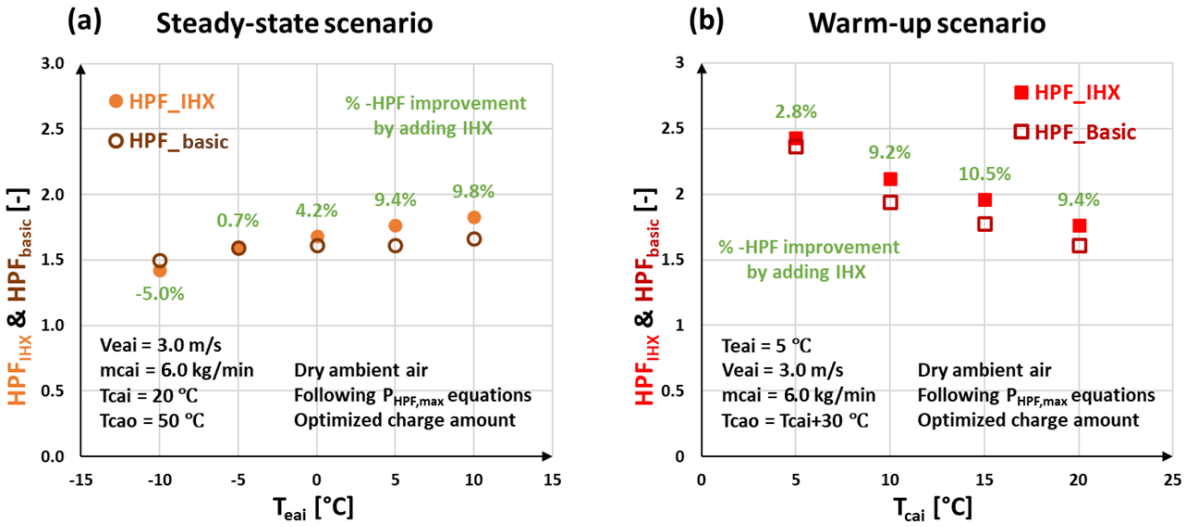

Figure 4: The performance data and benefits of IHX in steady-state and warm-up scenarios

The introduction of the IHX to the HP system not only yields higher energy performance but can also contributes to a safer operation of the system. It is known that the low side of the IHX prevents the liquid refrigerant from entering the compressor by heat exchanging with gas cooler exiting refrigerant. In addition, it has been experimentally confirmed in this paper that a system with IHX operates with higher evaporating temperatures than a basic system. **Figure 5(a)** and **(b)** show the evaporating temperatures for both basic and IHX systems for both steady-state and warm-up scenarios. Evaporating temperatures are compared to the dew point temperature T_{dpei}. The larger difference between the evaporating temperature and T_{dpei} would lead to faster frosting of the outdoor coil surface. IHX could not fully prevent frosting, especially at the lower ambient temperatures, but it can delay frost growing in the most demanding conditions when T_{eai} is between 0 to 5°C. Evaporating temperatures increase faster with T_{eai} and T_{cai} for the IHX system than for the basic system. The difference between those two could increase up to 6.1°C. However, at the ambient temperature T_{eai} = 0°C, the evaporating temperature can be higher up to 2.3°C.

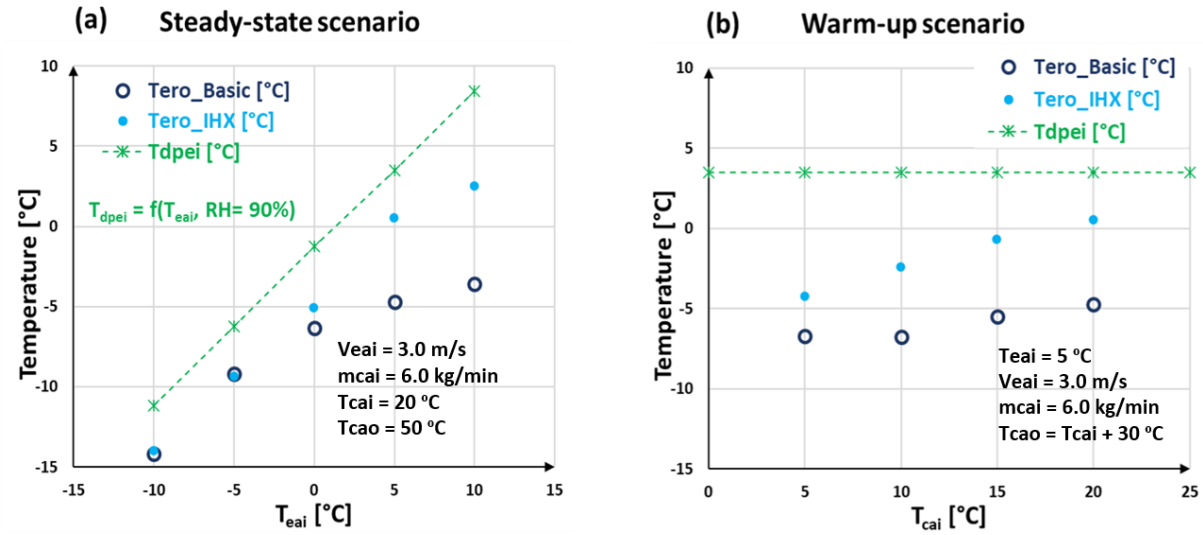

Figure 5: The performance data and benefits of IHX in frosting conditions

4. CONCLUSIONS

An R744 heat pump system was built to study the role of IHX in the transcritical mode experimentally. The results show:

- The IHX system requires the same refrigerant charge amount as the basic system at the defined conditions: T_{eai}= 0°C, T_{cai} = 10°C. The system is more stable in the work and less sensitive to a possible refrigerant leak.
- Introducing IHX does not change $P_{HPF,max}$ much, but the equation line has smaller slope in comparison to the basic system.
- IHX has a negligible effect on system efficiency when the HP system is operating with lower T_{eai}, due to compressor limitations. While it improves the system efficiency by up to 10.5% when the HP system is operating in transcritical mode with higher ambient temperature conditions.
- Introducing IHX reduces frosting on the outdoor coil due to a higher evaporating temperature. The evaporating temperature of the IHX system can be higher than it is for the basic system by up to 2.3°C, when the outdoor air temperature is 0°C.

NOMENCLATURE

AC	air-conditioning	$\dot{m}_r$	mass flow rate [kg/s]
Acc	accumulator	**OCR**	Oil Circulation Rate [-]
DP	differential pressure [Pa]	**P**	pressure [bar]
EXV	electronic expansion valve	**Q**	capacity [kW]
h	enthalpy [kJ/kg-°C]	**SH**	superheat [°C]
HP	heat pump	**T**	temperature [°C]
HPF	Heating Performance Factor	**V**	velocity [m/s]
IHX	internal heat exchanger	**W**	power [kW]
M	mass [kg]	**x**	quality [-]

Subscript

a/ air	air-side	i	inlet
acc	accumulator	id	indoor
c	Condenser/ gas cooler	n	nozzle
cham	Chamber-side	o	outlet
cp/ comp	compressor	od	outdoor
e	evaporator	oi	oil inlet
elec	electricity	oo	oil outlet
high	high-pressure side	r/ ref	refrigerant-side
g	glycol	x	expansion valve

REFERENCES

Cao, F., Ye, Z., & Wang, Y. (2020). Experimental investigation on the influence of internal heat exchanger in a transcritical CO2 heat pump water heater. *Applied Thermal Engineering, 168*, 114855. https://doi.org/10.1016/j.applthermaleng.2019.114855

Fernandez, N., Hwang, Y., & Radermacher, R. (2010). Comparison of CO2 heat pump water heater performance with baseline cycle and two high COP cycles. *International Journal of Refrigeration, 33(3)*, 635-644. https://doi.org/10.1016/j.ijrefrig.2009.12.008

Ghazizade-Ahsaee, H., & Ameri, M. (2018). Effects of using expander and internal heat exchanger on carbon dioxide direct-expansion geothermal heat pump. *Applied Thermal Engineering, 136*, 389-407. https://doi.org/10.1016/j.applthermaleng.2018.03.032

Inokuty, H. (1928). Graphical Method of finding compression pressure of CO2 refrigerating machine for maximum coefficient of performance. *Proceedings of the 5th IIR International Congress of Refrigeration*, 185–192.

Jung, J., Jeon, Y., Cho, W., & Kim, Y. (2020). Effects of injection-port angle and internal heat exchanger length in vapor injection heat pumps for electric vehicles. *Energy, 193*, 116751. https://doi.org/10.1016/j.energy.2019.116751

Junqi, D., Yibiao, W., Shiwei, J., Xianhui, Z., & Linjie, H. (2021). Experimental study of R744 heat pump system for electric vehicle application. *Applied Thermal Engineering, 183, Part 1*, 116191. https://doi.org/10.1016/j.applthermaleng.2020.116191

Kim, S. G., Kim, Y. J., Lee, G., & Kim, M. S. (2005). The performance of a transcritical CO2 cycle with an internal heat exchanger for hot water heating. *International Journal of Refrigeration*, *28*(7), 1064–1072. https://doi.org/10.1016/j.ijrefrig.2005.03.004

Kwan, T. H., Shen, Y., Wu, Z., & Yao, Q. (2020). Performance analysis of the thermoelectric device as the internal heat exchanger of the trans-critical carbon dioxide cycle. *Energy Conversion and Management, 208*, 112585. https://doi.org/10.1016/j.enconman.2020.112585

Lemmon, E.W., Huber, M.L., McLinden, M. O. (2010). *NIST Standard Reference Database 23: Reference Fluid Thermodynamic and Transport Properties-REFPROP, Version 9.0*. National Institute of Standards and Technology, Standard Reference Data Program.

Moffat, R. J. (1988). Describing the uncertainties in experimental results. *Experimental Thermal and Fluid Science*, *1*(1), 3–17.

Nguyen, A., Eslami-Nejad, P., Badache, M., & Bastani, A. (2019). Influence of an internal heat exchanger on the operation of a CO2 direct expansion ground source heat pump. *Energy and Buildings, 202*, 109343. https://doi.org/10.1016/j.enbuild.2019.109343

Ortega, I., Sieres, J., Cerdeira, F., Alvarez, E., & Rodriguez, J. (2019). Performance analysis of a R407C liquid-to-water heat pump: Effect of a liquid–vapor heat exchanger and domestic hot water production. *International Journal of Refrigeration, 101*, 125-135. https://doi.org/10.1016/j.ijrefrig.2019.02.024

Qin, X., Wang, D., Jin, Z., Wang, J., Zhang, G., & Li, H. (2021). A comprehensive investigation on the effect of internal heat exchanger based on a novel evaluation method in the transcritical CO2 heat pump system. *Renewable Energy, 178*, 574-586. https://doi.org/10.1016/j.renene.2021.06.082

Wang, Y., Ye, Z., Yin, X., Song, Y., & Cao, F. (2021). Energy, exergy and exergoeconomic evaluation of the air source transcritical CO2 heat pump with internal heat exchanger for space heating. *International Journal of Refrigeration, 130*, 14-26. https://doi.org/10.1016/j.ijrefrig.2021.06.028

Ye, Z., Wang, Y., Song, Y., Yin, X., Cao, F. (2020). Optimal discharge pressure in transcritical CO2 heat pump water heater with internal heat exchanger based on pinch point analysis. *International Journal of Refrigeration, 118*, 12-20. https://doi.org/10.1016/j.ijrefrig.2020.06.003

Zhang, W., Cernicin, V., & Hrnjak, P. (2022). The role of internal heat exchanger in an R744 vapor compression system in the air-conditioning mode under various conditions. *International Refrigeration and Air Conditioning Conference.*, No.2151.

ACKNOWLEDGEMENT

This work was supported by all members of ACRC at the University of Illinois at Urbana-Champaign. All the help from our members are gratefully acknowledged!